Atmos. Chem. Phys. Discuss., https://doi.org/10.5194/acp-2019-14
Manuscript under review for journal Atmos. Chem. Phys.
Discussion started: 16 January 2019

Atmospheric Chemistry and Physics Discussions

Significant source of secondary aerosol: formation from gasoline evaporation emissions in the presence of SO_2 and NH_3

Tianzeng Chen[1, 3, a], Yongchun Liu[2, a], Qingxin Ma[1, 3, 4, *], Biwu Chu[1, 3, 4], Peng Zhang [1], Changgeng Liu[1], Jun Liu[1, 3], Hong He[1, 3, 4, *]

[1] State Key Joint Laboratory of Environment Simulation and Pollution Control, Research Center for Eco-Environmental Sciences, Chinese Academy of Sciences, Beijing 100085, China

[2] Beijing Advanced Innovation center for Soft Matter Science and Engineering, Beijing University of Chemical Technology, Beijing 100029, China

[3] University of Chinese Academy of Sciences, Beijing 100049, China

[4] Center for Excellence in Regional Atmospheric Environment, Institute of Urban Environment, Chinese Academy of Sciences, Xiamen 361021, China

[a] These authors contributed equally to this work and should be considered as co-first authors

Corresponding authors: qxma@rcees.ac.cn (Qingxin Ma), and honghe@rcees.ac.cn (Hong He)

Atmos. Chem. Phys. Discuss., https://doi.org/10.5194/acp-2019-14
Manuscript under review for journal Atmos. Chem. Phys.
Discussion started: 16 January 2019

Atmospheric Chemistry and Physics Discussions

Abstract

Gasoline evaporation emissions have become an important anthropogenic source of urban atmospheric VOCs and secondary organic aerosol (SOA). These emissions have a significant impact on regional air quality, especially in China where car ownership is growing rapidly. However, the contribution of evaporation emissions on the secondary aerosol (SA) is not clear in air pollution complex in which high concentration of SO_2 and NH_3 was present. In this study, the effects of SO_2 and NH_3 on SA formation from unburned gasoline vapors were investigated in a 30 m^3 indoor smog chamber. It was found that increase in SO_2 and NH_3 concentrations could promote linearly the formation of SA, which could be enhanced by a factor of 1.6−2.6 and 2.0−2.5, respectively. Sulfate was most sensitive to the SO_2 concentration, followed by organic aerosol, which was due not only to the well-known acid catalytic effect, but also related to the formation of organic sulfur-containing compounds. In the case of increasing NH_3 concentration, ammonium nitrate increased more significantly than organic aerosol, and nitrogen-containing organics were also enhanced, as revealed by the results of positive matrix factorization (PMF) analysis. Meanwhile, new particle formation (NPF) and particle size growth were significantly enhanced in the presence of SO_2 and NH_3. This work indicates that gasoline evaporation emissions will be a significant source of SA, especially in the presence of high concentrations of SO_2 and NH_3. Meanwhile, these emissions might also be a potential source of sulfur- and nitrogen-containing organics. Our work provides a scientific basis for the synergistic emission reduction of secondary aerosol precursors, including NO_x, SO_2, NH_3 and particularly VOCs, to mitigate PM pollution in China.

Keywords

Secondary inorganic aerosol; Secondary organic aerosol; Sulfur dioxide; Ammonia; Sulfur-

Atmos. Chem. Phys. Discuss., https://doi.org/10.5194/acp-2019-14
Manuscript under review for journal Atmos. Chem. Phys.
Discussion started: 16 January 2019

containing organics; Nitrogen-containing organics

Atmos. Chem. Phys. Discuss., https://doi.org/10.5194/acp-2019-14
Manuscript under review for journal Atmos. Chem. Phys.
Discussion started: 16 January 2019

Atmospheric Chemistry and Physics Discussions

1 Introduction

Many areas in China such as the Beijing - Tianjin - Hebei region (BTH), Yangtze River Delta (YRD), Sichuan Basin and Pearl River Delta (PRD) are suffering from severe haze events (Li et al., 2017; Sun et al., 2016; Shen et al., 2015; He et al., 2014; Huang et al., 2014; Guo et al., 2014; Tan et al., 2009). Haze pollution has attracted widespread attention in recent years because of its adverse effects on human health, climate change and visibility (Thalman et al., 2017; Davidson et al., 2005; Pöschl, 2005).

During the haze events, high concentrations of SO_2, NH_3, and volatile organic compounds (VOCs) have always been observed (Zou et al., 2015; Liu et al., 2013; Meng et al., 2011; Yang et al., 2009), which are the precursors of secondary aerosol. Although the emission of SO_2 has decreased continuously since 2005 (Lu et al., 2010), China is still the largest contributor of SO_2 emissions in the world, mainly owing to the great demand for coal combustion (Bauduin et al., 2016). Also, high concentrations of SO_2 of more than 100 ppb (parts per billion) have been observed in northern China, especially during the heating period (Hou et al., 2016; Tong et al., 2016; Yang et al., 2009). As for atmospheric NH_3, as an alkaline inorganic gas, its main emission source is agricultural practices in China (Zhang et al., 2018; Fu et al., 2015). It has also been reported that vehicle exhaust also contributes to NH_3 emission in the urban areas (Sun et al., 2017). Sometimes, high concentrations of NH_3 of up to 100 ppb have been observed in Beijing, China (Ianniello et al., 2010). With respect to VOCs, it is well known that aromatics from anthropogenic sources (especially vehicle-related sources in urban areas) are critical secondary organic aerosol (SOA) precursors (Liu et al., 2015a; Gordon et al., 2014; Platt et al., 2013; Calvert et al., 2002). These aromatics could react with oxidants (e.g., O_3, OH, and NO_3 radicals), and undergo multi-step oxidative processes to form multifunctional products, which have sufficiently low volatility to contribute to SOA via gas-particle partitioning (Hallquist et al., 2009; Atkinson and Arey, 2003).

Research has shown that secondary aerosol (SA) makes a significant contribution (30−77%) to $PM_{2.5}$ during the severe haze events in China (Huang et al., 2014; Guo et al., 2014; Jimenez et al., 2009). However, there still exists a significant gap between the predicted SA derived from the current atmospheric quality models and that observed in field observations (Zhao et al., 2018; Yang et al., 2018; Zheng et al., 2015). Therefore, considering the characteristics of complex pollution in China, it is crucial to study the synergistic effects of SO_2 and NH_3 on the formation of SA, which might be an outstanding source of SA formation (Zhao et al., 2018; Chu et al., 2016; Liu et al., 2016; Santiago et al., 2012; Na et al., 2007).

A few studies have focused on the influence of SO_2 or NH_3 on SA formation. It has been found that SO_2 promotes SA formation from typical biogenic (e.g., isoprene and α-pinene) and anthropogenic (e.g., toluene, o-xylene, 1,3,5-trimethylbenzene, and gasoline vehicle exhaust) precursors through acid-catalyzed reactions (Chu et al., 2016; Liu et al., 2016; Lin et al., 2013; Santiago et al., 2012; Jaoui et al., 2008; Kleindienst et al., 2006; Edney et al., 2005), which promote the reactive uptake process of organic species or enhance the formation of high-molecular-weight compounds (Liggio and Li, 2008; Liggio et al., 2007; Liggio and Li, 2006). With regard to the role of NH_3 in SA formation, knowledge is still limited. Meanwhile, inconsistent impacts of NH_3 on SA formation have been reported under different precursor systems. For example, NH_3 could elevate SA formation in the α-pinene/ozone oxidation system through acid-base reactions (Na et al., 2007), while the effects of NH_3 neutralization were masked by other multiple factors and did not show significant influence on isoprene-derived SOA formation (Lin et al., 2013), and addition of NH_3 even significantly reduced the SA formation in the styrene/ozone system, which was caused by nucleophilic attack from the NH_3 molecule leading to rapid decomposition of the major aerosol products (Na et al., 2006). For the photo-oxidation of aromatic VOCs (e.g., toluene, o-/m-/p-xylene), the presence of NH_3 could facilitate new particle formation (NPF) and particle growth, subsequently leading to increased SA

formation (Li et al., 2018; Liu et al., 2015b).

At the present time, the effects of SO_2 and NH_3 on SA formation have rarely been studied under highly complex pollution conditions (Chu et al., 2016). Meanwhile, vehicular evaporation emissions have been reported to be non-negligible contributors (39.20 %) to ambient VOCs from anthropogenic sources compared with vehicular tailpipe emissions (Liu et al., 2017a). Therefore, it is necessary to study the influence of SO_2 and NH_3 on SA formation from evaporation emissions.

In this study, unburned gasoline vapors were used as a substitute for evaporative emissions, and the roles of SO_2 and NH_3 on SA formation from the photo-oxidation of unburned gasoline vapors were investigated in a 30 m^3 indoor smog chamber, in order to understand the formation potential of SA from oxidation of gasoline vapor in the cocktail of pollutants in Beijing. The respective influences of SO_2 and NH_3 on both the microphysics and chemistry of SA formation were examined. Meanwhile, the chemical compositions of the formed SOA in the presence of SO_2 and NH_3 were further explored by applying positive matrix factorization (PMF) analysis. The formation potentials of SA, sulfur- and nitrogen-containing organics from vehicular evaporation emissions in the presence of SO_2 and NH_3 were evaluated and discussed.

2 Materials and Methods

2.1 Gasoline fuel

The utilized gasoline fuel with grade 92# was collected (refer to the standard Method for manual sampling of petroleum liquids (GB/T 4756-2015)) from a gas station located in Beijing. The gasoline complies with the China V gasoline fuel standard. It contains 22.8 % (v/v) aromatics (mainly including benzene, toluene, xylene, trimethylbenzene) and 12.1 % (v/v) olefins. The composition of the gasoline is similar to the gasoline collected in North China reported by Tang et al. (2015) and could represent the gasoline used in most areas of China for studying SA formation potential. Details of the gasoline composition

are given in Table S1.

2.2 Smog chamber facility

A series of photochemical experiments with unburned gasoline vapors in the absence or presence of SO_2 or NH_3 were performed in a 30 m^3 indoor smog chamber at the Research Center for Eco-Environmental Sciences, Chinese Academy of Sciences (RCEES-CAS). The detailed schematic structure of the indoor smog chamber is given in Fig. S1 and described elsewhere (Chen et al., 2018). Briefly, the cuboid chamber reactor (L × W × H = 3.0 × 2.5 × 4.0 m, S/V = 1.97 m^{-1}) was irradiated by 120 UV lamps (Philips) with peak intensity at 365 nm, providing a NO_2 photolysis rate of 0.55 min^{-1}. The interior was coated with 125 μm-thick FEP100 film (DuPont™, US) and the chamber was located in a temperature-controlled room, in which the temperature (T) and relative humidity (RH) could be controlled mechanically. Meanwhile, a three-wing stainless-steel fan coated with Teflon was installed inside the reactor to guarantee that the gas and particle phase species mix sufficiently before photochemical reaction.

The chamber was also equipped with a series of gas- and particle-phase monitoring instruments. For gaseous NO_x, O_3 and SO_2, a chemiluminescence NO_x analyzer (Model 42i-TL, Thermo Fisher Scientific, USA), a UV photometric O_3 analyzer (Model 49i, Thermo Fisher Scientific, USA) and a pulsed fluorescence SO_2 analyzer (Model 43i, Thermo Fisher Scientific, USA) were used to monitor the concentrations in real time, respectively. The VOC species in gasoline were measured with a gas chromatograph (7890B GC, Agilent, USA) equipped with a DB-624 column (60 m × 0.25 mm × 1.40 μm, Agilent, USA) and a mass spectrometry detector (5977A MS, Agilent, USA) (GC-MS). In addition, high-resolution time-of-flight proton transfer reaction mass spectrometry (HR-ToF-PTRMS) (Ionicon Analytik GmbH, Austria) was also used for the measurement of gas-phase hydrocarbons and their intermediate products. The size distribution and number concentration of the formed particulate matter (PM) were measured using a scanning mobility

125 particle sizer (SMPS, TSI, USA), which was composed of a differential mobility analyzer (DMA, 3080
126 Classifier, TSI, USA) coupled with a condensation particle counter (CPC, 3776, TSI, USA). The mass
127 concentration was estimated based on the volume concentration and the density of PM calculated from the
128 equation $\rho = d_{va}/d_m$, where d_{va} is the mean vacuum aerodynamic diameter measured by an Aerodyne High-
129 Resolution Time-of-Flight Aerosol Mass Spectrometer (HR-ToF-AMS) and d_m is the mean electrical
130 mobility diameter measured by SMPS (DeCarlo et al., 2004). The calculated density of PM ranged from 1.5
131 to 1.6 g cm^{-3} in the different reaction systems. The mass concentration and chemical composition of PM
132 were simultaneously monitored using a high-resolution time-of-flight aerosol mass spectrometer (HR-ToF-
133 AMS, Aerodyne Research Inc. USA). Meanwhile, T and RH were monitored real-time using a hydro-
134 thermometer (Vaisala HMP110) during the entirety of each experiment.

135 **2.3 Wall loss corrections**

136 The measured particle concentration was corrected in accordance with the relationship between the
137 deposition rate (k_{dep}) and particle diameter (D_p, nm) (i.e., $k_{dep} = 4.15 \times 10^{-7} \times D_p^{1.89} + 1.39 \times D_p^{-0.88}$), which
138 was described by Takekawa et al. (2003). The wall loss rates of NO_2, NO, O_3 and VOC species were
139 determined to be $(1.67 \pm 0.25) \times 10^{-4}$, $(1.32 \pm 0.32) \times 10^{-4}$, $(3.32 \pm 0.21) \times 10^{-4}$ and $(2.20 \pm 0.39) \times 10^{-4}$ min^{-1}
140 , respectively. Therefore, the wall loss of gas phase species was evaluated to be less than 5% of their
141 maximum concentration in our study.

142 Wall losses of semi-volatile organic compounds (SVOCs) and low-volatility organic compounds
143 (LVOCs) would lead to a substantial underestimation of SA formation (Krechmer et al., 2016; Ye et al., 2016;
144 Zhang et al., 2015; Zhang et al., 2014), which is caused by the competition between these vapors condensing
145 onto particles versus onto chamber walls. This competition could be evaluated by the corresponding
146 timescales associated with reaching gas-to-particle partitioning equilibrium ($\overline{\tau}_{g\text{-}p}$) and vapor wall loss ($\tau_{g\text{-}w}$)

(Zhang et al., 2014), and this underestimation of SA formation could be approximately quantified by the ratio of these two timescales (i.e., $\bar{\tau}_{g\text{-}p}/\tau_{g\text{-}w}$). According to the methods described by Zhang et al. (2014), $\bar{\tau}_{g\text{-}p}$ and $\tau_{g\text{-}w}$ could be estimated assuming an upper bound and a lower bound of the molecular mass of organic vapors (MW) (100−300 g mol^{-1}) (as discussed in Supporting Information). In order to accurately quantify the SA formation, the underestimation caused by the loss of SVOCs and LVOCs (include sulfuric acid gas) to the chamber walls was taken into account in this study. In our study, the SA yields were underestimated by a factor of 1.97−2.82 fold when considering the ratio of these two timescales (i.e., $\bar{\tau}_{g\text{-}p}/\tau_{g\text{-}w}$), which showed a decreasing trend with the increase of the SO_2 and NH_3 initial concentrations, suggesting that an increasing proportion of vapors is partitioned onto the suspended particle surface rather than the chamber wall.

2.4 Experimental conditions

Prior to each experiment, the chamber reactor was flushed by purified and dry zero air for about 24−36 h at a flow rate of 100 L min^{-1} until almost no gas-phase species (i.e., NO_x, O_3 and SO_2) could be detected (< 1 ppb) and the particle number concentration was < 10 cm^{-3}. Before the experiments, the chamber was humidified to ~50 % RH by passing purified zero air through ultra-pure water (18.2 MΩ, Millipore Milli-Q). After that, a known volume of liquid gasoline (100 μL) was injected into the chamber through a heated Teflon line system (~100 °C) carried by purified dry zero air to ensure that all were evaporated into the chamber. Subsequently, NO_x, SO_2 or/and NH_3 were successively injected into the chamber from standard gas cylinders using mass flow controllers. The initial VOCs/NO_x ratio (ppbC/ppb) was kept constant (Table 1). In order to reduce the adsorption of NH_3 in the pipeline, the NH_3 flow in a bypass line was balanced for about 30 min before it was injected into the chamber. The concentrations of NO_x and SO_2 were continuously monitored until they were stable, ensuring that the gaseous species mixed well in the chamber. For the

Atmos. Chem. Phys. Discuss., https://doi.org/10.5194/acp-2019-14
Manuscript under review for journal Atmos. Chem. Phys.
Discussion started: 16 January 2019

concentration of NH_3, the value was estimated according to the amount of NH_3 introduced and the volume of the reactor chamber. The experiment was then conducted for about 8 h after turning off the fan and turning on the UV lights. All the experiments were performed at a temperature of 26 ± 1 °C and wet conditions (RH = 50 ± 3 %). The detailed experimental conditions are listed in Table 1. The letters in the abbreviations represent the reactants introduced into the chamber reactor for each experiment. For example, SGN is an experiment with the presence of sulfur dioxide (S), gasoline vapor (G), and nitrogen oxides (N). Four experiments (Exps. SGN1, SGN2, SGN3, and SGN4) were carried out at different SO_2 initial concentrations. AGN is an experiment with the presence of ammonia (A), gasoline vapor (G), and nitrogen oxides (N). Two experiments (Exps. AGN1 and AGN2) were carried out at different NH_3 initial concentrations.

3 Results and discussion

3.1 Effect of SO_2 and NH_3 on the gas-phase precursors

Time-resolved concentrations of inorganic and organic gas-phase species during the photo-oxidation of gasoline/NO_x in the absence or presence of SO_2 and NH_3 are shown in Fig. S2 and Fig. S3, respectively. After turning on the UV lights, NO was rapidly converted to NO_2. At the same time, O_3 was gradually generated, with a maximum concentration of up to 350 ppb (Fig. S2). As shown in Fig. S2, there was no obvious difference in the variation of NO_x and O_3 in the presence of SO_2 or NH_3. Meanwhile, the decay of typical VOC precursors (e.g., benzene, toluene) measured by HR-ToF-PTRMS is given in Fig. S3, which traced very closely with the GC-MS results (Fig. S4). There were also no observable differences in these VOCs among these experiments. According to the decay curves of aromatic hydrocarbons, the OH radical concentrations were estimated to be (7.54−8.40) × 10^6 molecules cm^{-3}, which were also similar among these experiments. In addition, the typical mass spectra of organic gas-phase species derived from HR-ToF-PTRMS after 480 min of the photo-oxidation reaction at different concentrations of SO_2 or NH_3 are shown

in Fig. S5, and no significant differences were found. Therefore, it is reasonable to deduce that the presence of SO_2 or NH_3 did not significantly impact the initial gas-phase oxidation mechanism of gasoline. This was consistent with the previous study conducted by Chu et al. (2016), who found that the presence of SO_2 and NH_3 did not significantly impact the initial gas-phase oxidation of toluene in the presence of NO_x.

3.2 Role of SO_2 in secondary aerosol formation

To investigate the effects of SO_2 on SA formation from the photo-oxidation of gasoline/NO_x, smog chamber experiments with different SO_2 initial concentrations were carried out (Table 1). As shown in Fig. 1, compared to the experiments without the addition of SO_2, the SA concentration was enhanced to different degrees (1.6−2.6 times) in the presence of different SO_2 concentrations (35−151 ppb, i.e., 100−431 μg m^{-3}). As for each chemical species (i.e., organics, nitrate, sulfate, and ammonium), they all showed a trend of linear increase with the increase of SO_2 concentration (Fig. 2), which indicated that aerosol formation will be significantly promoted by the existence of SO_2, especially for the sulfate and organic aerosol. Previous studies have also revealed its promoting role on SA formation from different precursors (Zhao et al., 2018; Liu et al., 2017b; Díaz-de-Mera et al., 2017; Liu et al., 2016; Chu et al., 2016). In addition, it is worth noting that ammonium aerosols were formed without the addition of gaseous NH_3 (Fig. S6), which indicated that some NH_3 was present in the background air in the chamber (Liu et al., 2015c). According to the concentration of generated ammonium aerosols, the concentration of background NH_3 was estimated to be ~15 ppb using the E-AIM model (Clegg and Brimblecombe, 2005; Wexler and Clegg, 2002; Clegg et al., 1998). Therefore, for the experiments with the presence of NH_3, the concentration of injected NH_3 (150−200 ppb) was much higher than this value to identify the effect of NH_3 on SA formation.

Additionally, the particle number concentrations and size growth were greatly enhanced by the presence of SO_2. As evident from Fig. 3, the corresponding maximal particle number concentrations (5.82×10^4−1.91

213 × 10^5 # cm^{-3}) were significantly enhanced by a factor of 2.9−3.3 in the presence of SO_2. This universal
214 phenomenon has been reported by many studies (Díaz-de-Mera et al., 2017; Liu et al., 2017b; Liu et al.,
215 2016; Chu et al., 2016). For example, the maximal particle number concentrations were enhanced by one
216 order of magnitude in the presence of SO_2 (~130 ppb) in the photo-oxidation of high concentration
217 toluene/NO_x (Chu et al., 2016). For complex precursor systems, Liu et al. (2016) have also found that under
218 high SO_2 concentration (~150 ppb) conditions, the maximum particle number concentrations increased by
219 5.4−48 times compared to those without SO_2 during the photo-oxidation of gasoline vehicle exhaust. In
220 addition, size distributions of generated SA in smaller size ranges (4−160 nm) were also determined using
221 another SMPS equipped with a nanometer differential mobility analyzer (Nano-DMA), indicating that the
222 new particle formation (NPF) phenomenon was enhanced significantly when the SO_2 concentration
223 increased (Fig. S7). The presence of high concentrations of SO_2 would generate sulfuric acid (H_2SO_4), which
224 would contribute to nucleation and increase the total particle number concentrations (Zhao et al., 2018; Sipilä
225 et al., 2010). Meanwhile, as the SO_2 concentration increased from 35 ppb to 151 ppb, the maximal particle
226 diameters (144−172 nm) became larger, which will have a direct impact on the scattering and absorption of
227 light (Seinfeld and Pandis, 2016). An enhancement effect of SO_2 on the surface area of particles was also
228 observed. As shown in Table 1, the surface area of aerosol particles at the end of each experiment increased
229 from 1.12 × 10^3 to 2.46 × 10^3 μm^2 cm^{-3} when the SO_2 concentration increased from 0 to 151 ppb. The larger
230 surface area would be beneficial to the condensation and heterogeneous uptake of low-volatility vapors
231 (Chapleski et al., 2016), consequently leading to higher SA yield in the presence of SO_2 (Table 1) (Santiago
232 et al., 2012).

233 In order to further investigate the role of SO_2 in the chemistry of SOA formation, the particle acidities
234 were estimated using the E-AIM model (Model II: H^+ - NH_4^+ - SO_4^{2-} - NO_3^- - H_2O) (Clegg and Brimblecombe,

2005; Wexler and Clegg, 2002; Clegg et al., 1998). The concentrations of chemical components (i.e., NH_4^+, SO_4^{2-}, and NO_3^-) at the time when the SOA formation rate reached its peak were used as the inputs of the model. As shown in Fig. 4, the H^+ concentration was increased from 8.5 to 32.5 nmol m^{-3} with the increase of SO_2 concentration under moderate humidity conditions (RH = 50 %) and the higher SOA concentration and SOA yield could be well explained by the enhancement of the particle acidities (R^2 = 0.960 and R^2 = 0.986, respectively). This phenomenon was related to the well-known acid-catalyzed reactions of multifunctional aldehydes (e.g., glyoxal and methylglyoxal), which were the products of aromatic hydrocarbons in the gasoline vapors through the gas-phase photo-oxidation. Previous studies have reported that hemiacetals, acetals and alcohols could be generated through the acid-catalyzed heterogeneous reactions of glyoxal (Czoschke et al., 2003; Jang et al., 2002). These low-vapor-pressure products preferentially partition into the particle phase and subsequently contribute to the SOA formation (Cao and Jang, 2007; Casale et al., 2007; Jang et al., 2002).

In addition, the sulfur-containing organics formed in the presence of SO_2 might be another reason for the increase of SOA yield (Kundu et al., 2013; Liggio et al., 2005). According to the linear fitting between the concentration of formed SO_4^{2-} and the amount of consumed SO_2 (after wall loss correction for SO_2, sulfuric acid gas and sulfate), there was a large gap between the slope of the line and the ratio of $M(SO_4^{2-})$ and $M(SO_2)$, as shown in Fig. S8. There are some possible reasons for this, including the underestimation of deposition and heterogeneous reaction of sulfur species on the wall, the formation of organic sulfur-containing products, and small leaks of pollutants from the smog chamber. Jaoui et al. (2008) also reported that the acidic aerosol generated in the presence of SO_2 could lead to sulfur-incorporating reactions in the particle phase during the photo-oxidation of α-pinene/toluene/NO_x mixtures. Sulfur-containing organics could be generated via reactions of organic species (e.g., polycyclic aromatic hydrocarbons (PAHs),

C10−C12 alkanes, alcohols, epoxides) with sulfate, bisulfate or sulfuric acid, especially under high relative humidity and acidity conditions (Riva et al., 2015, 2016; Huang et al., 2015; Hatch et al., 2011; Surratt et al., 2007; Liggio et al., 2005). Huang et al. (2015) have revealed that sulfur-containing organics with R-O-SO_3^- functional groups will yield S-bearing organic fragments ($C_xH_yO_zS$) during ionization, which subsequently could be detected by HR-ToF-AMS and used as marker ions to quantify them. In our gasoline/NO_x experiments in the presence of SO_2, the ions CSO^+, $CH_3SO_2^+$ and $CH_3SO_3^+$ could be separated (Fig. S9), although uncertainty might be induced in the peak-fitting of the highly abundant ions $C_2H_4O_2^+$, $C_6H_7^+$, and $C_5H_3O_2^+$. These characteristic ions (i.e., CSO^+, $CH_3SO_2^+$ and $CH_3SO_3^+$) also have been observed from sulfur-containing organics in previous field measurements (Huang et al., 2015; Farmer et al., 2010). According to the estimation method for sulfur-containing organics mentioned in Huang et al. (2015), we found that the signal of these ions and the concentrations of sulfur-containing organics increased with the SO_2 initial concentration (Fig. 5). The estimated concentrations of sulfur-containing organics (13−26 ng m^{-3}) were comparable to those (~ 20 ng m^{-3}) observed in the mid-Atlantic United States, which were derived from biogenic and anthropogenic hydrocarbons (Meade et al., 2016). Therefore, photo-oxidation of gasoline vapor in the presence of SO_2 might be a noteworthy source of sulfur-containing organics, although the concentration was very low compared to that of generated SO_4^{2-} (~ 0.1% of SO_4^{2-}).

3.3 Role of NH_3 in secondary aerosol formation

Similarly, the role of NH_3 in SA formation was examined. The SA concentration was enhanced by a factor of 2.0−2.5 in the presence of NH_3, as shown in Fig. S10a. The formation of SOA, NO_3^- and NH_4^+ was enhanced to varying degrees. The increase of NO_3^- and NH_4^+ could be attributed to the formation of inorganic NH_4NO_3 in the presence of NH_3. The NO^+/NO_2^+ ratio, which could be derived from HR-ToF-AMS, has often been used as a proxy for identification of inorganic nitrate and organic nitrogen compounds (Farmer

et al., 2010; Sato et al., 2010; Rollins et al., 2009). Generally, the NO^+/NO_2^+ ratio of inorganic nitrate (1.08−2.81) is lower than that of organic nitrogen compounds (3.82−5.84) (Liu et al., 2016). In this study, the NO^+/NO_2^+ ratio became substantially lower (~ 2.00) in the presence of NH_3 compared with that in the absence of NH_3 (~ 5.46). This phenomenon further indicated that NH_4NO_3 became a dominant nitrate species in the presence of NH_3. As for the reason for SOA enhancement, the presence of NH_3 could react with some organic acids and subsequently contribute to SOA formation (Na et al., 2007; Na et al., 2006), which could be supported by the increase of N/C (from 0.016 to 0.033) with increasing NH_3 concentration at similar concentrations of NO_x. This result indicated that NH_3 was incorporated in the photo-oxidation of gasoline vapor. In addition, we have found that the presence of NH_3 readily increased the particle diameter and number concentration of SA generated in the photo-oxidation of gasoline (Figs. S10b and S10c). These phenomena indicated that NH_3 played an important role in new particle formation (NPF). These results are consistent with the simulation results finding that NH_3 promotes atmospheric NPF and also the conversion of SO_2 and NO_2 (Jiang and Xia, 2017). Meanwhile, increased surface area of particles was also observed (Table 1, 2.07×10^3 and 2.48×10^3 μm^2 cm^{-3}) as the NH_3 concentration increased from 0 to 150 and 200 ppb. Similarly, the larger surface area would favor the partitioning of low-volatility vapors to the particle phase, leading to the higher SA yield (Table 1).

Previous studies have reported that the reaction of carbonyl compounds (e.g., glyoxal) could be catalyzed by NH_4^+ ions through a Bronsted acid pathway or an iminium pathway, which could generate N-containing products and oligomers (Nozière et al., 2009). It has been reported that nitrogen-containing organics could contribute a substantial fraction to SOA (Liu et al., 2015c; Farmer et al., 2010; Cheng et al., 2006). Previous researchers have identified the characteristic fragments of nitrogen-containing organics as $C_xH_yN_n$ and $C_xH_yO_zN_n$ using HR-ToF-AMS (Lee et al., 2013; Farmer et al., 2010; Galloway et al., 2009).

In our study, the typical normalized mass spectrum of N-containing fragments in SOA after 480 min of photo-oxidation reaction at different concentrations of NH_3 are given in Fig. 6. The prominent peaks in the $C_xH_yN_n$ family were at *m/z* 27 (CHN^+), 30 (CH_4N^+), 40($C_2H_2N^+$), 41(CHN_2^+, $C_2H_3N^+$), 42($C_2H_4N^+$), 43($C_2H_5N^+$), 54($C_2H_2N_2^+$, $C_3H_4N^+$), 55($C_3H_5N^+$), and 68($C_3H_4N_2^+$, $C_4H_6N^+$); and the $C_xH_yO_zN_n$ fragments were dominated by 45(CH_3ON^+), 46(CH_4ON^+), 59($C_2H_5ON^+$), 63($CH_5O_2N^+$), 73($C_2H_5ON_2^+$, $C_3H_7ON^+$), 86($C_3H_4O_2N^+$, $C_3H_6ON_2^+$), 91($C_3H_9O_2N^+$), 97($C_4H_5ON_2^+$), and 104($C_3H_6O_3N^+$, $C_4H_{10}O_2N^+$). The N-containing fragments observed in the experiment without added NH_3 could be attributed to the reactions between organic peroxy (RO_2) radicals and NO_x (Arey et al., 2001) or uptake of background NH_3 by SOA. Additionally, it was obvious that the signal intensities of most N-containing fragments became significantly stronger as the NH_3 concentration increased (150−200 ppb). Therefore, a considerable amount of nitrogen-containing organics (the ratio of nitrogen-containing organics to SOA was about 6.7−7.7%) was formed during the photo-oxidation of gasoline vapor in the presence of NH_3. This was consistent with the previous study conducted by Liu et al. (2015c), who observed the formation of organic nitrogen compounds in the SOA generated from the OH oxidation of m-xylene (Liu et al., 2015c). Meanwhile, the promoting role of NH_3 in the formation of N-containing species was also observed in the reaction system of ozonolysis and photo-oxidation of α-pinene (Babar et al., 2017).

In addition, elemental analysis was also carried out to elucidate the SOA chemical composition and SOA formation mechanisms (Chhabra et al., 2011; Heald et al., 2010) at different concentrations of NH_3. The time evolution of H/C and O/C in SOA formed from the photo-oxidation of gasoline vapor at different concentrations of NH_3 is shown in Fig. 7. As evident from Fig. 7, all data points are located in the triangular area for slope between -1 and 0, which suggests that SOA formation from the photo-oxidation of gasoline vapor is a combination of carboxylic acid and alcohol/peroxide (Heald et al., 2010). Meanwhile, in the

presence of NH_3, as shown in Fig. 8, N/C increased as reaction proceeded in the initial oxidation stage (0−120 min), accompanied by a rapid increase of O/C (0.12−0.67), a decrease of H/C (2.12−1.61), and a rapid formation of SOA. During this stage, the photo-oxidation of VOC precursors leads to a rapid increase in O/C and a rapid decrease in H/C. The termination chemistry of NO_x with free radicals and the NH_3 uptake result in a rapid increase in N/C. As the reaction proceeded further (120−300 min), an increase of H/C which should be caused by NH_3 uptake resulted in an almost constant oxidation state of SOA in the continuous photo-oxidation, accompanied by an increase in the SOA concentration. Nozière et al. (2009) have reported that N-containing products would be generated from carbonyl compound (e.g., glyoxal) self-reactions catalyzed by ammonium ions, which will have a dramatic impact on the volatility of oxidation products and the yield of SOA (Ortiz-Montalvo et al., 2014). In the last stage of the reaction (360−480 min), NH_3 uptake might reach saturation; therefore, H/C and N/C are almost constant. Comparing experiments with different concentrations of NH_3, the average H/C shows an obvious increase (1.53−1.70) while the average O/C (0.70−0.78) shows a slight increase with the increase of NH_3 concentration (0−200 ppb), seen in Fig. S11. The slope in the Van Krevelen diagram shows a trend from slope = -1 to slope = 0 (Fig. S11), indicating that the formed carboxylic acid would further react with NH_3 via acid-base reaction to generate an ammonium salt of a carboxylate anion in the presence of NH_3 (Na et al., 2007). Meanwhile, Xu et al. (2018) recently found that imidazole products containing multiple oxygen atoms could be generated through heterogeneous reactions between NH_3 and carbonyl compounds (e.g., glyoxal) (Xu et al., 2018), which might also contribute to the increase in the O/C of the SOA.

3.4 Different roles of SO_2 and NH_3 in SOA chemical properties

The chemical properties of the SOA generated under the different concentration of SO_2 or NH_3 were further compared by applying positive matrix factorization (PMF) analysis to the HR-ToF-AMS data,

345 respectively (Chu et al., 2016; Liu et al., 2014). The details of PMF analysis are given in the Supporting
346 Information. For the experiments under different SO_2 concentration conditions (i.e., Exps. GN, SGN1, SGN2,
347 SGN3 and SGN4), two factors (Factor 1-S and Factor 2-S, Fig. S12a) were identified from the PMF analysis,
348 and the difference mass spectra (*m/z* 12−170) between the two factors and the time series of the mass
349 concentrations are shown in Fig. 9. The intensity of C_xH_y and S-bearing organic fragments ($C_xH_yO_zS$) in
350 Factor 1-S was obviously stronger than that in Factor 2-S. Meanwhile, fragments in the high *m/z* range (>
351 110 Da) were more abundant in Factor 1-S (Fig. 9a, marked in red box). By contrast, the fragments
352 containing oxygen in Factor 2-S were more abundant than in Factor 1-S, such as the typical fragment CO_2^+
353 (*m/z* 44). Therefore, Factor 1-S was tentatively assigned to the less-oxygenated organic aerosol and
354 oligomers, while Factor 2-S was more-oxygenated organic aerosol (Ulbrich et al., 2009). Similarly, for the
355 experiments at different NH_3 concentration (i.e., Exps. GN, AGN1 and AGN2), two factors (Factor 1-N and
356 Factor 2-N, Fig. S12b) were also identified in the same way. According to Fig. 10, Factor 1-N was tentatively
357 assigned to the less-oxygenated organic aerosol and oligomers, while Factor 2-N was more-oxygenated
358 organic aerosol and nitrogen-containing organics.

359 As shown in Fig. 9b and Fig. 10b, these two factors both had different time series during the entire
360 reaction. With respect to Exps. GN, SGN1, SGN2, SGN3 and SGN4, Factor 1-S was formed later (~ 30 min)
361 than Factor 2-S, and then continuously increased during the entire reaction. Comparing experiments with
362 different SO_2 concentrations, the maximum concentration of Factor 1-S, which was related to the less-
363 oxygenated organic aerosol and oligomers, was enhanced with increased SO_2 concentration ($R^2 = 0.881$, Fig.
364 9c). This suggested that the presence of SO_2 was prone to decrease the oxidation state of organic aerosol via
365 acid-catalyzed reactions and enhance the formation of oligomers (Liu et al., 2016), which was consistent
366 with the evolution of O/C vs. H/C shown in Fig. S13. Meanwhile, the gradually increasing concentration of

Factor 1-S was related to the formation of sulfur-containing organics in the presence of SO_2 (Blair et al., 2017). By contrast, Factor 2-S was first gradually increased with the progress of the reaction and then decreased after reaching a peak (i.e., inflection point). Meanwhile, the time to reach the inflection point was affected by the SO_2 concentration (Fig. 9b). As the initial concentration of SO_2 increased from 0 ppb to 151 ppb, the time corresponding to the inflection point decreased, which indicated that the adverse influence of acid catalysis on Factor 2-S was gradually enhanced. In addition, the maximum concentration of Factor 2-S was negatively related with SO_2 concentration (R^2 = 0.987, Fig. 9c); this suggested that the presence of SO_2 and acid catalysis was adverse to the formation of more-oxygenated organic aerosol, leading to the decrease of the oxidation state of organic aerosol (Fig. S13).

By contrast, for Exps. GN, AGN1 and AGN2, Factor 1-N was first increased with the progress of the reaction and then gradually decreased after reaching a peak (Fig. 10b); while Factor 2-N was formed later (~ 30 min) than Factor 1-N, and then continuously increased during the entire reaction. This phenomenon was consistent with the expected behavior, that less-oxidized organic aerosol would be further oxidized to form more-oxidized organic aerosol. When comparing experiments with different NH_3 concentrations, it was observed that the concentration of Factor 1-N increased with increasing NH_3 concentration. Meanwhile, Factor 1-N, which was related to the more-oxidized organic aerosol and nitrogen-containing organics, was a dominant factor in the presence of NH_3, and its maximum concentration was enhanced with the increase in NH_3 concentration (R^2 = 0.988, Fig. 10c). This phenomenon indicated that the formation of more-oxygenated organic aerosol and nitrogen-containing organics was enhanced with the increase of NH_3 concentration. Meanwhile, a negative correlation was observed between the maximum concentration of Factor 1-N and NH_3 concentration (R^2 = 0.876, Fig. 10c); this revealed that less-oxygenated organic aerosol was gradually transformed to highly oxidized species and nitrogen-containing organics in the presence of

NH_3.

4 Conclusions

In our study, SA formation from the photo-oxidation of gasoline/NO_x in the presence of SO_2 or NH_3 was investigated. Our experimental results suggested that SA was enhanced by a factor of 1.6−2.6 or 2.0−2.5, respectively, with the increase of SO_2 or NH_3 concentration (0−151 ppb and 0−200 ppb, respectively). Meanwhile, both secondary organic aerosol (SOA) and secondary inorganic aerosol (SIA) could be increased by varying degrees. In the presence of SO_2, SO_4^{2-} showed the most sensitive linear increase trend with the increase of SO_2 concentration ($k = 8.4\times10^{-2}$), and SOA was also greatly enhanced ($k = 2.9\times10^{-2}$) by the well-known acid catalytic effect and the formation of sulfur-containing organics. In the presence of NH_3, NH_4NO_3 was most enhanced, following by organic aerosol. The formation of nitrogen-containing organics, which were identified by applying PMF analysis, was also promoted by the presence of NH_3. Meanwhile, conspicuous new particle formation (NPF) and particle size growth were observed in the presence of SO_2 or NH_3.

Our results indicate that the photo-oxidation of gasoline/NO_x in the presence of SO_2 and NH_3 is a significant source of SA. Therefore, in order to mitigate $PM_{2.5}$ pollution in China, emission control strategies should not only pay attention to primary particulate emissions, but also focus on synergistic reduction of the emission of SA precursors including NO_x, SO_2, NH_3 and, particularly, VOCs. In this study, a linear relationship was observed between the SA yield and SO_2 or NH_3 concentration (Fig. S14). In recent years, vehicular evaporation emissions have gradually attracted attention due to their non-negligible contribution (39.20 %, 1.65 Tg yr^{-1}) to ambient VOCs (Liu et al., 2017a). Considering the typical concentrations of SO_2 and NH_3 of 40 ppb and 23 ppb in haze pollution in the north China plain (Cheng et al., 2016), the SA yield is roughly estimated to be about 0.3. Then, the SA formed from the photo-oxidation of VOCs emitted by

411 vehicular evaporation in the presence of SO_2 and NH_3 is roughly estimated to be 0.49 Tg yr^{-1}, which is about
412 twice as much as the primary $PM_{2.5}$ emissions from transportation (0.21 Tg in 2007) in China (Jing et al.,
413 2015; Zhang et al., 2007). This estimate indicates that vehicular evaporation emissions will be a significant
414 source of SA in the presence of SO_2 and NH_3, although the estimate might have a high uncertainty due to
415 the fact that SA yield might vary considerably under different atmospheric conditions. Meanwhile, in the
416 presence of NO_x, SO_2 and NH_3, vehicular evaporation emissions might be a potential source of sulfur- and
417 nitrogen-containing organics, according to the results obtained from our study. Previous studies have
418 indicated that sulfur- and nitrogen-containing organics have an adverse influence on the climate by light
419 absorption and/or by affecting aerosol hygroscopicity (Staudt et al., 2014; Nguyen et al., 2012), and they
420 also have a significant contribution to SOA and nitrogen or sulfur budgets (Lee et al., 2016; Shang et al.,
421 2016).

422 Therefore, more attention should be paid to collaborative control reductions in vehicular evaporation
423 emissions and gaseous pollutants, including NO_x, SO_2, and NH_3. This will contribute to reducing the burden
424 of $PM_{2.5}$, and then cut the environmental, economic and health costs caused by PM pollution. Corresponding
425 emission controls should be taken into consideration by policy makers for future management. Our work
426 will provide a scientific basis for taking corresponding control measures to relieve haze events in China.
427 Additionally, further work should be focused on SA formation from vehicular evaporation under coexisting
428 SO_2 and NH_3 conditions to shed light on the formation mechanism of SA under more atmospherically
429 relevant conditions.

430 ## Author contributions

431 HH, QXM, YCL, and TZC proposed the initial idea. YCL and TZC designed and led the study. YCL,
432 BWC, QXM, PZ, and TZC conducted the data analyses. TZC, YCL, BWC, PZ, CGL, and JL interpreted the

data. TZC, YCL, JL, and QXM wrote the manuscript, with inputs from all coauthors.

Acknowledgements

This work was financially supported by the National Key R&D Program of China (2016YFC0202700, 2018YFC0506901), the National Natural Science Foundation of China (41877306, 41877304, 21876185, and 91744205), the special fund of the State Key Joint Laboratory of Environment Simulation and Pollution Control (17L01ESPC), the Youth Innovation Promotion Association, CAS (2018060, 2018055, and 2017064) and Key Research Program of Frontier Sciences, CAS (QYZDB-SSW-DQC018).

References

Arey, J., Aschmann, S. M., Kwok, E. S. C., and Atkinson, R.: Alkyl nitrate, hydroxyalkyl nitrate, and hydroxycarbonyl formation from the NO_x−air photooxidations of C_5−C_8 n-alkanes, J. Phys. Chem. A, 105, 1020-1027, doi: 10.1021/jp003292z, 2001.

Atkinson, R., and Arey, J.: Atmospheric degradation of volatile organic compounds, Chem. Rev., 103, 4605-4638, doi: 10.1021/cr0206420, 2003.

Babar, Z. B., Park, J.-H., and Lim, H.-J.: Influence of NH_3 on secondary organic aerosols from the ozonolysis and photooxidation of α-pinene in a flow reactor, Atmos. Environ., 164, 71-84, doi: 10.1016/j.atmosenv.2017.05.034, 2017.

Bauduin, S., Clarisse, L., Hadji-Lazaro, J., Theys, N., Clerbaux, C., and Coheur, P. F.: Retrieval of near-surface sulfur dioxide (SO_2) concentrations at a global scale using IASI satellite observations, Atmo. Meas. Tech., 9, 721-740, doi: 10.5194/amt-9-721-2016, 2016.

Blair, S. L., MacMillan, A. C., Drozd, G. T., Goldstein, A. H., Chu, R. K., Paša-Tolić, L., Shaw, J. B., Tolić, N., Lin, P., Laskin, J., Laskin, A., and Nizkorodov, S. A.: Molecular characterization of organosulfur compounds in biodiesel and diesel fuel secondary organic aerosol, Environ. Sci. Technol., 51, 119-127, doi:

10.1021/acs.est.6b03304, 2017.

Calvert, J. G., Atkinson, R., Becker, K. H., Kamens, R. M., Seinfeld, J. H., Wallington, T. H., and Yarwood, G.: The mechanisms of atmospheric oxidation of the aromatic hydrocarbons, Oxford University Press, 2002.

Cao, G., and Jang, M.: Effects of particle acidity and UV light on secondary organic aerosol formation from oxidation of aromatics in the absence of NO_x, Atmos. Environ., 41, 7603-7613, doi: 10.1016/j.atmosenv.2007.05.034, 2007.

Casale, M. T., Richman, A. R., Elrod, M. J., Garland, R. M., Beaver, M. R., and Tolbert, M. A.: Kinetics of acid-catalyzed aldol condensation reactions of aliphatic aldehydes, Atmos. Environ., 41, 6212-6224, doi: 10.1016/j.atmosenv.2007.04.002, 2007.

Chapleski, R. C., Zhang, Y., Troya, D., and Morris, J. R.: Heterogeneous chemistry and reaction dynamics of the atmospheric oxidants, O_3, NO_3, and OH, on organic surfaces, Chem. Soc. Rev., 45, 3731-3746, doi: 10.1039/C5CS00375J, 2016.

Chen, T., Liu, Y., Chu, B., Liu, C., Liu, J., Ge, Y., Ma, Q., Ma, J., and He, H.: Differences of the oxidation process and secondary organic aerosol formation at low and high precursor concentrations, J. Environ. Sci., doi: 10.1016/j.jes.2018.11.011, 2018.

Cheng, Y., Li, S.-M., and Leithead, A.: Chemical characteristics and origins of nitrogen-containing organic compounds in $PM_{2.5}$ aerosols in the Lower Fraser Valley, Environ. Sci. Technol., 40, 5846-5852, doi: 10.1021/es0603857, 2006.

Cheng, Y., Zheng, G., Wei, C., Mu, Q., Zheng, B., Wang, Z., Gao, M., Zhang, Q., He, K., Carmichael, G., Pöschl, U., and Su, H.: Reactive nitrogen chemistry in aerosol water as a source of sulfate during haze events in China, Sci. Adv., 2, doi: 10.1126/sciadv.1601530, 2016.

Chhabra, P. S., Ng, N. L., Canagaratna, M. R., Corrigan, A. L., Russell, L. M., Worsnop, D. R., Flagan, R.

C., and Seinfeld, J. H.: Elemental composition and oxidation of chamber organic aerosol, Atmos. Chem. Phys., 11, 8827-8845, doi: 10.5194/acp-11-8827-2011, 2011.

Chu, B., Zhang, X., Liu, Y., He, H., Sun, Y., Jiang, J., Li, J., and Hao, J.: Synergetic formation of secondary inorganic and organic aerosol: effect of SO_2 and NH_3 on particle formation and growth, Atmos. Chem. Phys., 16, 14219-14230, doi: 10.5194/acp-16-14219-2016, 2016.

Clegg, S. L., Brimblecombe, P., and Wexler, A. S.: Thermodynamic model of the system H^+–NH_4^+–SO_4^{2-}–NO_3^-–H_2O at tropospheric temperatures, J. Phys. Chem. A, 102, 2137-2154, doi: 10.1021/jp973042r, 1998.

Clegg, S. L., and Brimblecombe, P.: Comment on the "Thermodynamic Dissociation Constant of the Bisulfate Ion from Raman and Ion Interaction Modeling Studies of Aqueous Sulfuric Acid at Low Temperatures", J. Phys. Chem. A, 109, 2703-2706, doi: 10.1021/jp0401170, 2005.

Czoschke, N. M., Jang, M., and Kamens, R. M.: Effect of acidic seed on biogenic secondary organic aerosol growth, Atmos. Environ., 37, 4287-4299, doi: 10.1016/S1352-2310(03)00511-9, 2003.

Davidson, C. I., Phalen, R. F., and Solomon, P. A.: Airborne particulate matter and human health: a review, Aerosol Sci. Tech., 39, 737-749, doi: 10.1080/02786820500191348, 2005.

DeCarlo, P. F., Slowik, J. G., Worsnop, D. R., Davidovits, P., and Jimenez, J. L.: Particle morphology and density characterization by combined mobility and aerodynamic diameter measurements. Part 1: Theory, Aerosol Sci. Tech., 38, 1185-1205, doi: 10.1080/027868290903907, 2004.

Díaz-de-Mera, Y., Aranda, A., Martínez, E., Rodríguez, A. A., Rodríguez, D., and Rodríguez, A.: Formation of secondary aerosols from the ozonolysis of styrene: effect of SO_2 and H_2O, Atmos. Environ., 171, 25-31, doi: 10.1016/j.atmosenv.2017.10.011, 2017.

Edney, E. O., Kleindienst, T. E., Jaoui, M., Lewandowski, M., Offenberg, J. H., Wang, W., and Claeys, M.: Formation of 2-methyl tetrols and 2-methylglyceric acid in secondary organic aerosol from laboratory irradiated

499 isoprene/NO_x/SO_2/air mixtures and their detection in ambient $PM_{2.5}$ samples collected in the eastern United States,
500 Atmos. Environ., 39, 5281-5289, doi: 10.1016/j.atmosenv.2005.05.031, 2005.

501 Farmer, D. K., Matsunaga, A., Docherty, K. S., Surratt, J. D., Seinfeld, J. H., Ziemann, P. J., and Jimenez, J.
502 L.: Response of an aerosol mass spectrometer to organonitrates and organosulfates and implications for
503 atmospheric chemistry, Proc. Natl. Acad. Sci. USA, 107, 6670-6675, doi: 10.1073/pnas.0912340107, 2010.

504 Fu, X., Wang, S. X., Ran, L. M., Pleim, J. E., Cooter, E., Bash, J. O., Benson, V., and Hao, J. M.: Estimating
505 NH_3 emissions from agricultural fertilizer application in China using the bi-directional CMAQ model coupled to
506 an agro-ecosystem model, Atmos. Chem. Phys., 15, 6637-6649, doi: 10.5194/acp-15-6637-2015, 2015.

507 Galloway, M. M., Chhabra, P. S., Chan, A. W. H., Surratt, J. D., Flagan, R. C., Seinfeld, J. H., and Keutsch,
508 F. N.: Glyoxal uptake on ammonium sulphate seed aerosol: reaction products and reversibility of uptake under
509 dark and irradiated conditions, Atmos. Chem. Phys., 9, 3331-3345, doi: 10.5194/acp-9-3331-2009, 2009.

510 Gordon, T. D., Presto, A. A., May, A. A., Nguyen, N. T., Lipsky, E. M., Donahue, N. M., Gutierrez, A.,
511 Zhang, M., Maddox, C., Rieger, P., Chattopadhyay, S., Maldonado, H., Maricq, M. M., and Robinson, A. L.:
512 Secondary organic aerosol formation exceeds primary particulate matter emissions for light-duty gasoline vehicles,
513 Atmos. Chem. Phys., 14, 4661-4678, doi: 10.5194/acp-14-4661-2014, 2014.

514 Guo, S., Hu, M., Zamora, M. L., Peng, J., Shang, D., Zheng, J., Du, Z., Wu, Z., Shao, M., Zeng, L., Molina,
515 M. J., and Zhang, R.: Elucidating severe urban haze formation in China, Proc. Natl. Acad. Sci. USA, 111, 17373-
516 17378, doi: 10.1073/pnas.1419604111, 2014.

517 Hallquist, M., Wenger, J. C., Baltensperger, U., Rudich, Y., Simpson, D., Claeys, M., Dommen, J., Donahue,
518 N. M., George, C., Goldstein, A. H., Hamilton, J. F., Herrmann, H., Hoffmann, T., Iinuma, Y., Jang, M., Jenkin,
519 M. E., Jimenez, J. L., Kiendler-Scharr, A., Maenhaut, W., McFiggans, G., Mentel, T. F., Monod, A., Prévôt, A. S.
520 H., Seinfeld, J. H., Surratt, J. D., Szmigielski, R., and Wildt, J.: The formation, properties and impact of secondary

organic aerosol: current and emerging issues, Atmos. Chem. Phys., 9, 5155-5236, doi: 10.5194/acp-9-5155-2009, 2009.

Hatch, L. E., Creamean, J. M., Ault, A. P., Surratt, J. D., Chan, M. N., Seinfeld, J. H., Edgerton, E. S., Su, Y., and Prather, K. A.: Measurements of isoprene-derived organosulfates in ambient aerosols by aerosol time-of-flight mass spectrometry—Part 2: temporal variability and formation mechanisms, Environ. Sci. Technol., 45, 8648-8655, doi: 10.1021/es2011836, 2011.

He, H., Wang, Y., Ma, Q., Ma, J., Chu, B., Ji, D., Tang, G., Liu, C., Zhang, H., and Hao, J.: Mineral dust and NO_x promote the conversion of SO_2 to sulfate in heavy pollution days, Sci. Rep., 4, 4172, doi: 10.1038/srep04172, 2014.

Heald, C. L., Kroll, J. H., Jimenez, J. L., Docherty, K. S., DeCarlo, P. F., Aiken, A. C., Chen, Q., Martin, S. T., Farmer, D. K., and Artaxo, P.: A simplified description of the evolution of organic aerosol composition in the atmosphere, Geophys. Res. Lett., 37, L08803, doi: 10.1029/2010GL042737, 2010.

Hou, S., Tong, S., Ge, M., and An, J.: Comparison of atmospheric nitrous acid during severe haze and clean periods in Beijing, China, Atmos. Environ., 124, 199-206, doi: 10.1016/j.atmosenv.2015.06.023, 2016.

Huang, D. D., Li, Y. J., Lee, B. P., and Chan, C. K.: Analysis of organic sulfur compounds in atmospheric aerosols at the HKUST supersite in Hong Kong using HR-ToF-AMS, Environ. Sci. Technol., 49, 3672-3679, doi: 10.1021/es5056269, 2015.

Huang, R.-J., Zhang, Y., Bozzetti, C., Ho, K.-F., Cao, J.-J., Han, Y., Daellenbach, K. R., Slowik, J. G., Platt, S. M., Canonaco, F., Zotter, P., Wolf, R., Pieber, S. M., Bruns, E. A., Crippa, M., Ciarelli, G., Piazzalunga, A., Schwikowski, M., Abbaszade, G., Schnelle-Kreis, J., Zimmermann, R., An, Z., Szidat, S., Baltensperger, U., Haddad, I. E., and Prevot, A. S. H.: High secondary aerosol contribution to particulate pollution during haze events in China, Nature, 514, 218-222, doi: 10.1038/nature13774, 2014.

543 Ianniello, A., Spataro, F., Esposito, G., Allegrini, I., Rantica, E., Ancora, M. P., Hu, M., and Zhu, T.:
544 Occurrence of gas phase ammonia in the area of Beijing (China), Atmos. Chem. Phys., 10, 9487-9503, doi:
545 10.5194/acp-10-9487-2010, 2010.
546 Jang, M., Czoschke, N. M., Lee, S., and Kamens, R. M.: Heterogeneous atmospheric aerosol production by
547 acid-catalyzed particle-phase reactions, Science, 298, 814-817, doi: 10.1126/science.1075798, 2002.
548 Jaoui, M., Edney, E. O., Kleindienst, T. E., Lewandowski, M., Offenberg, J. H., Surratt, J. D., and Seinfeld,
549 J. H.: Formation of secondary organic aerosol from irradiated α-pinene/toluene/NO_x mixtures and the effect of
550 isoprene and sulfur dioxide, J. Geophys. Res., 113, doi: doi:10.1029/2007JD009426, 2008.
551 Jiang, B., and Xia, D.: Role identification of NH_3 in atmospheric secondary new particle formation in haze
552 occurrence of China, Atmos. Environ., 163, 107-117, doi: 10.1016/j.atmosenv.2017.05.035, 2017.
553 Jimenez, J. L., Canagaratna, M. R., Donahue, N. M., Prevot, A. S. H., Zhang, Q., Kroll, J. H., DeCarlo, P. F.,
554 Allan, J. D., Coe, H., Ng, N. L., Aiken, A. C., Docherty, K. S., Ulbrich, I. M., Grieshop, A. P., Robinson, A. L.,
555 Duplissy, J., Smith, J. D., Wilson, K. R., Lanz, V. A., Hueglin, C., Sun, Y. L., Tian, J., Laaksonen, A., Raatikainen,
556 T., Rautiainen, J., Vaattovaara, P., Ehn, M., Kulmala, M., Tomlinson, J. M., Collins, D. R., Cubison, M. J., Dunlea,
557 J., Huffman, J. A., Onasch, T. B., Alfarra, M. R., Williams, P. I., Bower, K., Kondo, Y., Schneider, J., Drewnick,
558 F., Borrmann, S., Weimer, S., Demerjian, K., Salcedo, D., Cottrell, L., Griffin, R., Takami, A., Miyoshi, T.,
559 Hatakeyama, S., Shimono, A., Sun, J. Y., Zhang, Y. M., Dzepina, K., Kimmel, J. R., Sueper, D., Jayne, J. T.,
560 Herndon, S. C., Trimborn, A. M., Williams, L. R., Wood, E. C., Middlebrook, A. M., Kolb, C. E., Baltensperger,
561 U., and Worsnop, D. R.: Evolution of organic aerosols in the atmosphere, Science, 326, 1525-1529, doi:
562 10.1126/science.1180353, 2009.
563 Jing, M., Junfeng, L., Yuan, X., and Shu, T.: Tracing primary $PM_{2.5}$ emissions via Chinese supply chains,
564 Environ. Res. Lett., 10, 054005, 2015.

565 Kleindienst, T. E., Edney, E. O., Lewandowski, M., Offenberg, J. H., and Jaoui, M.: Secondary organic
566 carbon and aerosol yields from the irradiations of isoprene and α-pinene in the presence of NO_x and SO_2, Environ.
567 Sci. Technol., 40, 3807-3812, doi: 10.1021/es052446r, 2006.
568 Krechmer, J. E., Pagonis, D., Ziemann, P. J., and Jimenez, J. L.: Quantification of gas-wall partitioning in
569 Teflon environmental chambers using rapid bursts of low-volatility oxidized species generated in situ, Environ.
570 Sci. Technol., 50, 5757-5765, doi: 10.1021/acs.est.6b00606, 2016.
571 Kroll, J. H., Donahue, N. M., Jimenez, J. L., Kessler, S. H., Canagaratna, M. R., Wilson, K. R., Altieri, K.
572 E., Mazzoleni, L. R., Wozniak, A. S., Bluhm, H., Mysak, E. R., Smith, J. D., Kolb, C. E., and Worsnop, D. R.:
573 Carbon oxidation state as a metric for describing the chemistry of atmospheric organic aerosol, Nat. Chem., 3,
574 133, doi: 10.1038/nchem.948, 2011.
575 Kundu, S., Quraishi, T. A., Yu, G., Suarez, C., Keutsch, F. N., and Stone, E. A.: Evidence and quantitation
576 of aromatic organosulfates in ambient aerosols in Lahore, Pakistan, Atmos. Chem. Phys., 13, 4865-4875, doi:
577 10.5194/acp-13-4865-2013, 2013.
578 Lee, A. K. Y., Zhao, R., Li, R., Liggio, J., Li, S.-M., and Abbatt, J. P. D.: Formation of light absorbing organo-
579 nitrogen species from evaporation of droplets containing glyoxal and ammonium sulfate, Environ. Sci. Technol.,
580 47, 12819-12826, doi: 10.1021/es402687w, 2013.
581 Lee, B. H., Mohr, C., Lopez-Hilfiker, F. D., Lutz, A., Hallquist, M., Lee, L., Romer, P., Cohen, R. C., Iyer,
582 S., Kurtén, T., Hu, W., Day, D. A., Campuzano-Jost, P., Jimenez, J. L., Xu, L., Ng, N. L., Guo, H., Weber, R. J.,
583 Wild, R. J., Brown, S. S., Koss, A., de Gouw, J., Olson, K., Goldstein, A. H., Seco, R., Kim, S., McAvey, K.,
584 Shepson, P. B., Starn, T., Baumann, K., Edgerton, E. S., Liu, J., Shilling, J. E., Miller, D. O., Brune, W.,
585 Schobesberger, S., D'Ambro, E. L., and Thornton, J. A.: Highly functionalized organic nitrates in the southeast
586 United States: Contribution to secondary organic aerosol and reactive nitrogen budgets, Proc. Natl. Acad. Sci.

587 USA, 113, 1516-1521, doi: 10.1073/pnas.1508108113, 2016.

588 Li, K., Chen, L., White, S. J., Yu, H., Wu, X., Gao, X., Azzi, M., and Cen, K.: Smog chamber study of the
589 role of NH3 in new particle formation from photo-oxidation of aromatic hydrocarbons, Sci. Total Environ., 619-
590 620, 927-937, doi: 10.1016/j.scitotenv.2017.11.180, 2018.

591 Li, L., Tan, Q., Zhang, Y., Feng, M., Qu, Y., An, J., and Liu, X.: Characteristics and source apportionment of
592 $PM_{2.5}$ during persistent extreme haze events in Chengdu, southwest China, Environ. Pollut., 230, 718-729, doi:
593 10.1016/j.envpol.2017.07.029, 2017.

594 Liggio, J., Li, S.-M., and McLaren, R.: Heterogeneous reactions of glyoxal on particulate matter:
595 identification of acetals and sulfate esters, Environ. Sci. Technol., 39, 1532-1541, doi: 10.1021/es048375y, 2005.

596 Liggio, J., and Li, S. M.: Reactive uptake of pinonaldehyde on acidic aerosols, J. Geophys. Res., 111, doi:
597 doi:10.1029/2005JD006978, 2006.

598 Liggio, J., Li, S. M., Brook, J. R., and Mihele, C.: Direct polymerization of isoprene and α-pinene on acidic
599 aerosols, Geophys. Res. Lett., 34, doi: doi:10.1029/2006GL028468, 2007.

600 Liggio, J., and Li, S. M.: Reversible and irreversible processing of biogenic olefins on acidic aerosols, Atmos.
601 Chem. Phys., 8, 2039-2055, doi: 10.5194/acp-8-2039-2008, 2008.

602 Lin, Y. H., Knipping, E. M., Edgerton, E. S., Shaw, S. L., and Surratt, J. D.: Investigating the influences of
603 SO_2 and NH_3 levels on isoprene-derived secondary organic aerosol formation using conditional sampling
604 approaches, Atmos. Chem. Phys., 13, 8457-8470, doi: 10.5194/acp-13-8457-2013, 2013.

605 Liu, H., Man, H., Cui, H., Wang, Y., Deng, F., Wang, Y., Yang, X., Xiao, Q., Zhang, Q., Ding, Y., and He, K.:
606 An updated emission inventory of vehicular VOCs and IVOCs in China, Atmos. Chem. Phys., 17, 12709-12724,
607 doi: 10.5194/acp-17-12709-2017, 2017a.

608 Liu, S., Jia, L., Xu, Y., Tsona, N. T., Ge, S., and Du, L.: Photooxidation of cyclohexene in the presence of

609 SO_2: SOA yield and chemical composition, Atmos. Chem. Phys., 17, 13329-13343, doi: 10.5194/acp-17-13329-
610 2017, 2017b.
611 Liu, T., Wang, X., Deng, W., Hu, Q., Ding, X., Zhang, Y., He, Q., Zhang, Z., Lü, S., Bi, X., Chen, J., and Yu,
612 J.: Secondary organic aerosol formation from photochemical aging of light-duty gasoline vehicle exhausts in a
613 smog chamber, Atmos. Chem. Phys., 15, 9049-9062, doi: 10.5194/acp-15-9049-2015, 2015a.
614 Liu, T., Wang, X., Deng, W., Zhang, Y., Chu, B., Ding, X., Hu, Q., He, H., and Hao, J.: Role of ammonia in
615 forming secondary aerosols from gasoline vehicle exhaust, Sci. China Chem., 58, 1377-1384, doi:
616 10.1007/s11426-015-5414-x, 2015b.
617 Liu, T., Wang, X., Hu, Q., Deng, W., Zhang, Y., Ding, X., Fu, X., Bernard, F., Zhang, Z., Lü, S., He, Q., Bi,
618 X., Chen, J., Sun, Y., Yu, J., Peng, P., Sheng, G., and Fu, J.: Formation of secondary aerosols from gasoline vehicle
619 exhaust when mixing with SO_2, Atmos. Chem. Phys., 16, 675-689, doi: 10.5194/acp-16-675-2016, 2016.
620 Liu, X. G., Li, J., Qu, Y., Han, T., Hou, L., Gu, J., Chen, C., Yang, Y., Liu, X., Yang, T., Zhang, Y., Tian, H.,
621 and Hu, M.: Formation and evolution mechanism of regional haze: a case study in the megacity Beijing, China,
622 Atmos. Chem. Phys., 13, 4501-4514, doi: 10.5194/acp-13-4501-2013, 2013.
623 Liu, Y., Li, S. M., and Liggio, J.: Technical Note: application of positive matrix factor analysis in
624 heterogeneous kinetics studies utilizing the mixed-phase relative rates technique, Atmos. Chem. Phys., 14, 9201-
625 9211, doi: 10.5194/acp-14-9201-2014, 2014.
626 Liu, Y., Liggio, J., Staebler, R., and Li, S. M.: Reactive uptake of ammonia to secondary organic aerosols:
627 kinetics of organonitrogen formation, Atmos. Chem. Phys., 15, 13569-13584, doi: 10.5194/acp-15-13569-2015,
628 2015c.
629 Lu, Z., Streets, D. G., Zhang, Q., Wang, S., Carmichael, G. R., Cheng, Y. F., Wei, C., Chin, M., Diehl, T.,
630 and Tan, Q.: Sulfur dioxide emissions in China and sulfur trends in East Asia since 2000, Atmos. Chem. Phys.,

10, 6311-6331, doi: 10.5194/acp-10-6311-2010, 2010.

Meade, L. E., Riva, M., Blomberg, M. Z., Brock, A. K., Qualters, E. M., Siejack, R. A., Ramakrishnan, K., Surratt, J. D., and Kautzman, K. E.: Seasonal variations of fine particulate organosulfates derived from biogenic and anthropogenic hydrocarbons in the mid-Atlantic United States, Atmos. Environ., 145, 405-414, doi: 10.1016/j.atmosenv.2016.09.028, 2016.

Meng, Z. Y., Lin, W. L., Jiang, X. M., Yan, P., Wang, Y., Zhang, Y. M., Jia, X. F., and Yu, X. L.: Characteristics of atmospheric ammonia over Beijing, China, Atmos. Chem. Phys., 11, 6139-6151, doi: 10.5194/acp-11-6139-2011, 2011.

Na, K., Song, C., and Cocker, D. R.: Formation of secondary organic aerosol from the reaction of styrene with ozone in the presence and absence of ammonia and water, Atmos. Environ., 40, 1889-1900, doi: 10.1016/j.atmosenv.2005.10.063, 2006.

Na, K., Song, C., Switzer, C., and Cocker, D. R.: Effect of ammonia on secondary organic aerosol formation from α-pinene ozonolysis in dry and humid conditions, Environ. Sci. Technol., 41, 6096-6102, doi: 10.1021/es061956y, 2007.

Nguyen, T. B., Lee, P. B., Updyke, K. M., Bones, D. L., Laskin, J., Laskin, A., and Nizkorodov, S. A.: Formation of nitrogen- and sulfur-containing light-absorbing compounds accelerated by evaporation of water from secondary organic aerosols, J. Geophys. Res., 117, doi: 10.1029/2011jd016944, 2012.

Nozière, B., Dziedzic, P., and Córdova, A.: Products and kinetics of the liquid-phase reaction of glyoxal catalyzed by ammonium ions (NH_4^+), J. Phys. Chem. A, 113, 231-237, doi: 10.1021/jp8078293, 2009.

Ortiz-Montalvo, D. L., Häkkinen, S. A. K., Schwier, A. N., Lim, Y. B., McNeill, V. F., and Turpin, B. J.: Ammonium addition (and aerosol pH) has a dramatic impact on the volatility and yield of glyoxal secondary organic aerosol, Environ. Sci. Technol., 48, 255-262, doi: 10.1021/es4035667, 2014.

653 Platt, S. M., El Haddad, I., Zardini, A. A., Clairotte, M., Astorga, C., Wolf, R., Slowik, J. G., Temime-Roussel,
654 B., Marchand, N., Ježek, I., Drinovec, L., Močnik, G., Möhler, O., Richter, R., Barmet, P., Bianchi, F.,
655 Baltensperger, U., and Prévôt, A. S. H.: Secondary organic aerosol formation from gasoline vehicle emissions in
656 a new mobile environmental reaction chamber, Atmos. Chem. Phys., 13, 9141-9158, doi: 10.5194/acp-13-9141-
657 2013, 2013.
658 Pöschl, U.: Atmospheric aerosols: composition, transformation, climate and health effects, Angew. Chem.
659 Int. Ed., 44, 7520-7540, doi: 10.1002/anie.200501122, 2005.
660 Riva, M., Tomaz, S., Cui, T., Lin, Y.-H., Perraudin, E., Gold, A., Stone, E. A., Villenave, E., and Surratt, J.
661 D.: Evidence for an unrecognized secondary anthropogenic source of organosulfates and sulfonates: gas-phase
662 oxidation of polycyclic aromatic hydrocarbons in the presence of sulfate aerosol, Environ. Sci. Technol., 49, 6654-
663 6664, doi: 10.1021/acs.est.5b00836, 2015.
664 Riva, M., Da Silva Barbosa, T., Lin, Y. H., Stone, E. A., Gold, A., and Surratt, J. D.: Chemical
665 characterization of organosulfates in secondary organic aerosol derived from the photooxidation of alkanes,
666 Atmos. Chem. Phys., 16, 11001-11018, doi: 10.5194/acp-16-11001-2016, 2016.
667 Rollins, A. W., Kiendler-Scharr, A., Fry, J. L., Brauers, T., Brown, S. S., Dorn, H. P., Dube, W. P., Fuchs, H.,
668 Mensah, A., Mentel, T. F., Rohrer, F., Tillmann, R., Wegener, R., Wooldridge, P. J., and Cohen, R. C.: Isoprene
669 oxidation by nitrate radical: Alkyl nitrate and secondary organic aerosol yields, Atmos. Chem. Phys., 9, 6685-
670 6703, doi: 10.5194/acp-9-6685-2009, 2009.
671 Santiago, M., Garcia Vivanco, M., and Stein, A. F.: SO_2 effect on secondary organic aerosol from a mixture
672 of anthropogenic VOCs: experimental and modelled results, Int. J. Environ. Pollut., 50, 224-233, 2012.
673 Sato, K., Takami, A., Isozaki, T., Hikida, T., Shimono, A., and Imamura, T.: Mass spectrometric study of
674 secondary organic aerosol formed from the photo-oxidation of aromatic hydrocarbons, Atmos. Environ., 44, 1080-

1087, doi: 10.1016/j.atmosenv.2009.12.013, 2010.

Seinfeld, J. H., and Pandis, S. N.: Atmospheric chemistry and physics: from air pollution to climate change, John Wiley & Sons, Hoboken, NJ, 2016.

Shang, J., Passananti, M., Dupart, Y., Ciuraru, R., Tinel, L., Rossignol, S., Perrier, S., Zhu, T., and George, C.: SO_2 uptake on oleic acid: a new formation pathway of organosulfur compounds in the atmosphere, Environ. Sci. Technol. Let., 3, 67-72, doi: 10.1021/acs.estlett.6b00006, 2016.

Shen, X. J., Sun, J. Y., Zhang, X. Y., Zhang, Y. M., Zhang, L., Che, H. C., Ma, Q. L., Yu, X. M., Yue, Y., and Zhang, Y. W.: Characterization of submicron aerosols and effect on visibility during a severe haze-fog episode in Yangtze River Delta, China, Atmos. Environ., 120, 307-316, doi: 10.1016/j.atmosenv.2015.09.011, 2015.

Sipilä, M., Berndt, T., Petäjä, T., Brus, D., Vanhanen, J., Stratmann, F., Patokoski, J., Mauldin, R. L., Hyvärinen, A.-P., Lihavainen, H., and Kulmala, M.: The role of sulfuric acid in atmospheric nucleation, Science, 327, 1243-1246, doi: 10.1126/science.1180315, 2010.

Staudt, S., Kundu, S., Lehmler, H.-J., He, X., Cui, T., Lin, Y.-H., Kristensen, K., Glasius, M., Zhang, X., Weber, R. J., Surratt, J. D., and Stone, E. A.: Aromatic organosulfates in atmospheric aerosols: synthesis, characterization, and abundance, Atmos. Environ., 94, 366-373, doi: 10.1016/j.atmosenv.2014.05.049, 2014.

Sun, K., Tao, L., Miller, D. J., Pan, D., Golston, L. M., Zondlo, M. A., Griffin, R. J., Wallace, H. W., Leong, Y. J., Yang, M. M., Zhang, Y., Mauzerall, D. L., and Zhu, T.: Vehicle emissions as an important urban ammonia source in the United States and China, Environ. Sci. Technol., 51, 2472-2481, doi: 10.1021/acs.est.6b02805, 2017.

Sun, Y., Chen, C., Zhang, Y., Xu, W., Zhou, L., Cheng, X., Zheng, H., Ji, D., Li, J., Tang, X., Fu, P., and Wang, Z.: Rapid formation and evolution of an extreme haze episode in Northern China during winter 2015, Sci. Rep., 6, 27151, doi: 10.1038/srep27151, 2016.

Surratt, J. D., Kroll, J. H., Kleindienst, T. E., Edney, E. O., Claeys, M., Sorooshian, A., Ng, N. L., Offenberg,

J. H., Lewandowski, M., Jaoui, M., Flagan, R. C., and Seinfeld, J. H.: Evidence for organosulfates in secondary organic aerosol, Environ. Sci. Technol., 41, 517-527, doi: 10.1021/es062081q, 2007.

Takekawa, H., Minoura, H., and Yamazaki, S.: Temperature dependence of secondary organic aerosol formation by photo-oxidation of hydrocarbons, Atmos. Environ., 37, 3413-3424, doi: 10.1016/S1352-2310(03)00359-5, 2003.

Tan, J.-H., Duan, J.-C., Chen, D.-H., Wang, X.-H., Guo, S.-J., Bi, X.-H., Sheng, G.-Y., He, K.-B., and Fu, J.-M.: Chemical characteristics of haze during summer and winter in Guangzhou, Atmos. Res., 94, 238-245, doi: 10.1016/j.atmosres.2009.05.016, 2009.

Tang, G., Sun, J., Wu, F., Sun, Y., Zhu, X., Geng, Y., and Wang, Y.: Organic composition of gasoline and its potential effects on air pollution in North China, Sci. China Chem., 58, 1416-1425, doi: 10.1007/s11426-015-5464-0, 2015.

Thalman, R., de Sá, S. S., Palm, B. B., Barbosa, H. M. J., Pöhlker, M. L., Alexander, M. L., Brito, J., Carbone, S., Castillo, P., Day, D. A., Kuang, C., Manzi, A., Ng, N. L., Sedlacek Iii, A. J., Souza, R., Springston, S., Watson, T., Pöhlker, C., Pöschl, U., Andreae, M. O., Artaxo, P., Jimenez, J. L., Martin, S. T., and Wang, J.: CCN activity and organic hygroscopicity of aerosols downwind of an urban region in central Amazonia: seasonal and diel variations and impact of anthropogenic emissions, Atmos. Chem. Phys., 17, 11779-11801, doi: 10.5194/acp-17-11779-2017, 2017.

Tong, S., Hou, S., Zhang, Y., Chu, B., Liu, Y., He, H., Zhao, P., and Ge, M.: Exploring the nitrous acid (HONO) formation mechanism in winter Beijing: direct emissions and heterogeneous production in urban and suburban areas, Faraday Discuss., 189, 213-230, doi: 10.1039/c5fd00163c, 2016.

Ulbrich, I. M., Canagaratna, M. R., Zhang, Q., Worsnop, D. R., and Jimenez, J. L.: Interpretation of organic components from positive matrix factorization of aerosol mass spectrometric data, Atmos. Chem. Phys., 9, 2891-

719 2918, doi: 10.5194/acp-9-2891-2009, 2009.

720 Wexler, A. S., and Clegg, S. L.: Atmospheric aerosol models for systems including the ions H^+, NH_4^+, Na^+,

721 SO_4^{2-}, NO_3^-, Cl^-, Br^-, and H_2O, J. Geophys. Res., 107, doi: 10.1029/2001jd000451, 2002.

722 Xu, J., Huang, M.-Q., Cai, S.-Y., Liao, Y.-M., Hu, C.-J., Zhao, W.-X., Gu, X.-J., and Zhang, W.-J.: Chemical

723 composition and reaction mechanisms for aged p-xylene secondary organic aerosol in the presence of ammonia,

724 J. Chin. Chem. Soc-taip, 65, 578-590, doi: doi:10.1002/jccs.201700249, 2018.

725 Yang, S., Yuesi, W., and Changchun, Z.: Measurement of the vertical profile of atmospheric SO_2 during the

726 heating period in Beijing on days of high air pollution, Atmos. Environ., 43, 468-472, doi:

727 10.1016/j.atmosenv.2008.09.057, 2009.

728 Yang, W., Li, J., Wang, M., Sun, Y., and Wang, Z.: A case study of investigating secondary organic aerosol

729 formation pathways in Beijing using an observation-based SOA Box Model, Aerosol Air Qual. Res., 18, 1606-

730 1616, doi: 10.4209/aaqr.2017.10.0415, 2018.

731 Ye, P., Ding, X., Hakala, J., Hofbauer, V., Robinson, E. S., and Donahue, N. M.: Vapor wall loss of semi-

732 volatile organic compounds in a Teflon chamber, Aerosol Sci. Tech., 50, 822-834, doi:

733 10.1080/02786826.2016.1195905, 2016.

734 Zhang, L., Chen, Y., Zhao, Y., Henze, D. K., Zhu, L., Song, Y., Paulot, F., Liu, X., Pan, Y., Lin, Y., and Huang,

735 B.: Agricultural ammonia emissions in China: reconciling bottom-up and top-down estimates, Atmos. Chem.

736 Phys., 18, 339-355, doi: 10.5194/acp-18-339-2018, 2018.

737 Zhang, Q., Streets, D. G., He, K., and Klimont, Z.: Major components of China's anthropogenic primary

738 particulate emissions, Environ. Res. Lett., 2, doi: 10.1088/1748-9326/2/4/045027, 2007.

739 Zhang, X., Cappa, C. D., Jathar, S. H., McVay, R. C., Ensberg, J. J., Kleeman, M. J., and Seinfeld, J. H.:

740 Influence of vapor wall loss in laboratory chambers on yields of secondary organic aerosol, Proc. Natl. Acad. Sci.

741 USA, 111, 5802-5807, doi: 10.1073/pnas.1404727111, 2014.

742 Zhang, X., Schwantes, R. H., McVay, R. C., Lignell, H., Coggon, M. M., Flagan, R. C., and Seinfeld, J. H.:
743 Vapor wall deposition in Teflon chambers, Atmos. Chem. Phys., 15, 4197-4214, doi: 10.5194/acp-15-4197-2015,
744 2015.

745 Zhao, D., Schmitt, S. H., Wang, M., Acir, I. H., Tillmann, R., Tan, Z., Novelli, A., Fuchs, H., Pullinen, I.,
746 Wegener, R., Rohrer, F., Wildt, J., Kiendler-Scharr, A., Wahner, A., and Mentel, T. F.: Effects of NO_x and SO_2 on
747 the secondary organic aerosol formation from photooxidation of α-pinene and limonene, Atmos. Chem. Phys., 18,
748 1611-1628, doi: 10.5194/acp-18-1611-2018, 2018.

749 Zhao, D., Song, X., Zhu, T., Zhang, Z., Liu, Y., and Shang, J.: Multiphase oxidation of SO_2 by NO_2 on $CaCO_3$
750 particles, Atmos. Chem. Phys., 18, 2481-2493, doi: 10.5194/acp-18-2481-2018, 2018.

751 Zheng, B., Zhang, Q., Zhang, Y., He, K. B., Wang, K., Zheng, G. J., Duan, F. K., Ma, Y. L., and Kimoto, T.:
752 Heterogeneous chemistry: a mechanism missing in current models to explain secondary inorganic aerosol
753 formation during the January 2013 haze episode in North China, Atmos. Chem. Phys., 15, 2031-2049, doi:
754 10.5194/acp-15-2031-2015, 2015.

755 Zou, Y., Deng, X. J., Zhu, D., Gong, D. C., Wang, H., Li, F., Tan, H. B., Deng, T., Mai, B. R., Liu, X. T., and
756 Wang, B. G.: Characteristics of 1 year of observational data of VOCs, NO_x and O_3 at a suburban site in Guangzhou,
757 China, Atmos. Chem. Phys., 15, 6625-6636, doi: 10.5194/acp-15-6625-2015, 2015.

Atmos. Chem. Phys. Discuss., https://doi.org/10.5194/acp-2019-14
Manuscript under review for journal Atmos. Chem. Phys.
Discussion started: 16 January 2019

Atmospheric Chemistry and Physics Discussions

758 Table 1. Summary of experimental conditions in this study.

Exp. [a]	RH (%)	T (°C)	SO_2 (ppb)	NH_3 [b] (ppb)	HC_0 (ppb)	$NO_{x,0}$ (ppb)	$HC_0/NO_{x,0}$ (ppbC ppb^{-1})	Surface [c] ($\mu m^2\ cm^{-3}$)	ΔHC ($\mu g\ m^{-3}$)	Δ*M* ($\mu g\ m^{-3}$)	SA yield [d]
GN	50±3	26±1	–	–	411.0	128.4	20.61	1.12×10^3	747.8	34.6	0.130
SGN1	50±3	26±1	35	–	419.8	121.0	22.34	1.73×10^3	871.6	58.0	0.155
SGN2	50±3	26±1	74	–	412.0	121.3	21.88	2.06×10^3	866.2	77.8	0.193
SGN3	50±3	26±1	116	–	383.6	119.8	20.62	2.23×10^3	791.1	87.1	0.226
SGN4	50±3	26±1	151	–	394.4	125.9	20.17	2.46×10^3	810.7	106.3	0.258
AGN1	50±3	26±1	–	150	413.8	120.4	22.12	1.79×10^3	700.6	47.6	0.158
AGN2	50±3	26±1	–	200	411.5	122.6	21.61	2.23×10^3	749.1	58.3	0.166

759 [a] Letters in abbreviations represent the reactants introduced into the chamber reactor, i.e., "G" represents
760 gasoline, "N" represents nitrogen oxides, "S" represents sulfur dioxide, "A" represents ammonia.
761 [b] The concentration of NH_3 is estimated by the amount of NH_3 added and the volume of the smog chamber.
762 [c] The surface area of aerosol particles measured by SMPS after 480 min of each experiment.
763 [d] SA yield was calculated after taking vapor and particle wall loss into account.

Atmos. Chem. Phys. Discuss., https://doi.org/10.5194/acp-2019-14
Manuscript under review for journal Atmos. Chem. Phys.
Discussion started: 16 January 2019

Atmospheric Chemistry and Physics Discussions

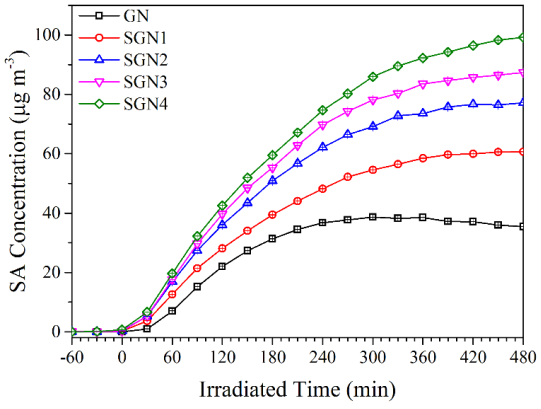

764

765 Fig. 1. Time series of secondary aerosol concentrations during the photo-oxidation experiments with different SO_2

766 concentrations (Exps. GN, SGN1, SGN2, SGN3, and SGN4).

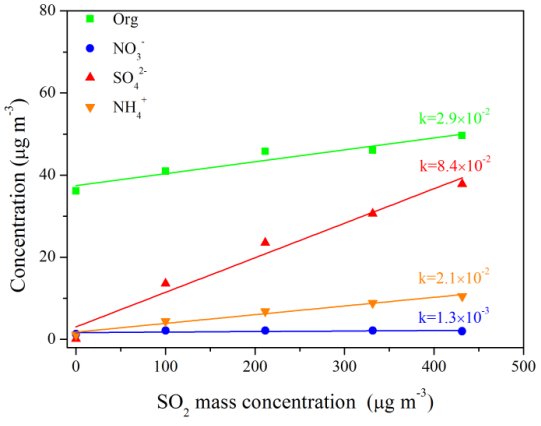

767

768 Fig. 2. Linear relationship between the concentration of chemical species (i.e., organic (green), nitrate (blue), sulfate (red), and

769 ammonium (orange)) and SO_2 under different SO_2 initial concentration conditions (Exps. GN, SGN1, SGN2, SGN3, and

770 SGN4). Each line represents a linear fitting and the k values are the corresponding slopes for each chemical species.

Atmos. Chem. Phys. Discuss., https://doi.org/10.5194/acp-2019-14
Manuscript under review for journal Atmos. Chem. Phys.
Discussion started: 16 January 2019

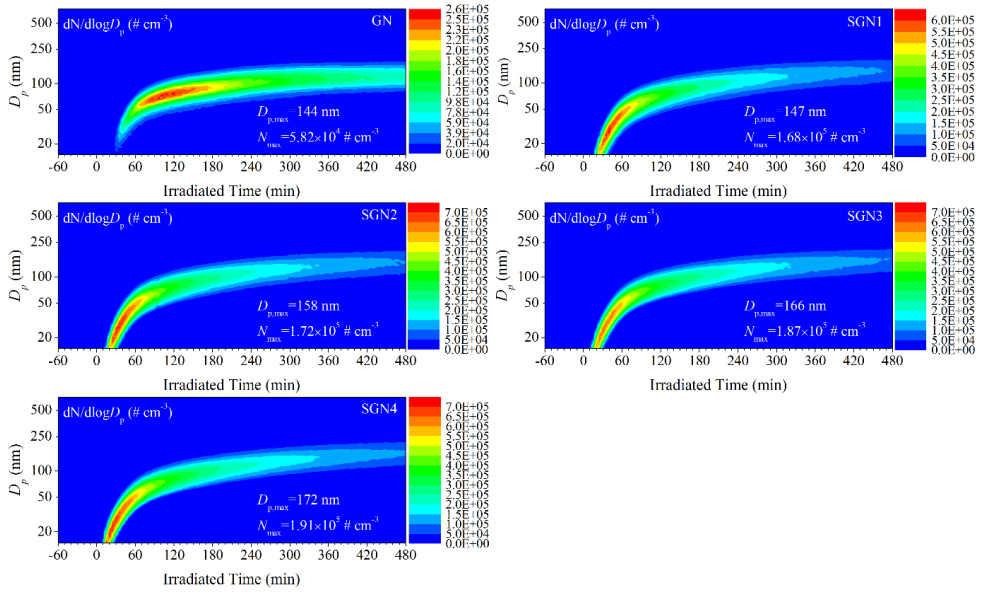

771

772 Fig. 3. Time series of the size distributions for the generated secondary aerosol during the photo-oxidation experiments with

773 different SO_2 initial concentrations (Exps. GN, SGN1, SGN2, SGN3, and SGN4). $D_{p,max}$ and N_{max} represent the maximal

774 diameter and number concentration of generated secondary aerosol, respectively, during each photo-oxidation experiment.

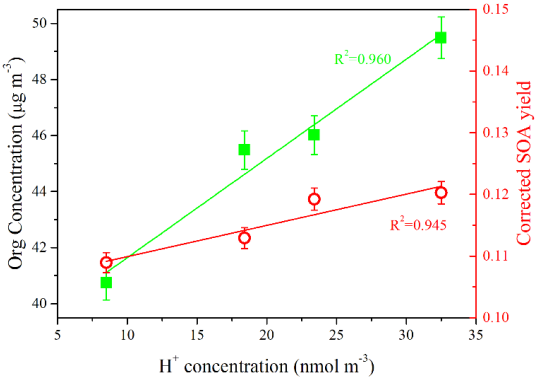

775

776 Fig. 4. Relationship between SOA concentration (left y axis), corrected SOA yield (right y axis) and H^+ concentration, which

777 was used to characterize the particle acidities. The H^+ concentration presented in this plot was the value when the SOA

778 formation rate reached the peak during each experiment (Exps. SGN1, SGN2, SGN3, and SGN4).

Atmos. Chem. Phys. Discuss., https://doi.org/10.5194/acp-2019-14
Manuscript under review for journal Atmos. Chem. Phys.
Discussion started: 16 January 2019

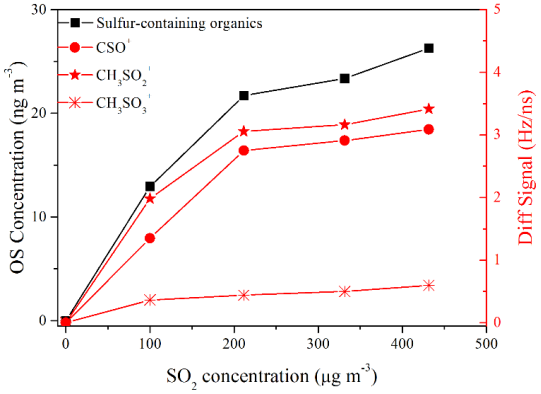

Fig. 5. Signal of fitted peaks, i.e., CSO^+, $CH_3SO_2^+$, $CH_3SO_3^+$ (right y axis) and sulfur-containing organics concentration (left y axis) as a function of SO_2 initial concentration.

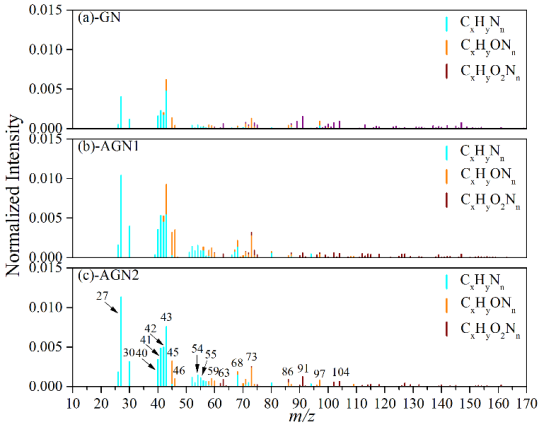

Fig. 6. Typical normalized mass spectra of N-containing fragments in SOA formed from the photo-oxidation of gasoline vapor at different concentrations of NH_3 (Exps. GN, AGN1 and AGN2).

Atmos. Chem. Phys. Discuss., https://doi.org/10.5194/acp-2019-14
Manuscript under review for journal Atmos. Chem. Phys.
Discussion started: 16 January 2019

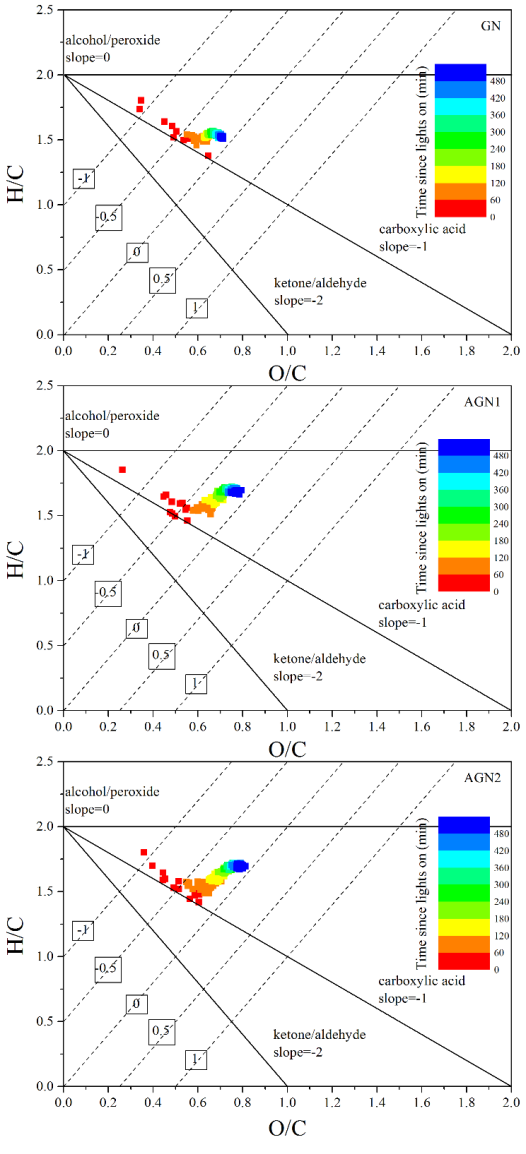

Fig. 7. Time evolution of H/C and O/C in SOA formed from the photo-oxidation of gasoline vapor at different concentrations of NH_3 (Exp. GN, AGN1 and AGN2). The numbers (i.e., -1, -0.5, 0, 0.5, and 1) labeling the dashed lines show the average carbon oxidation state (OSc = 2×O/C−H/C) (Kroll et al., 2011). The black lines represent the addition of functional groups to an aliphatic carbon (Heald et al., 2010).

Atmos. Chem. Phys. Discuss., https://doi.org/10.5194/acp-2019-14
Manuscript under review for journal Atmos. Chem. Phys.
Discussion started: 16 January 2019

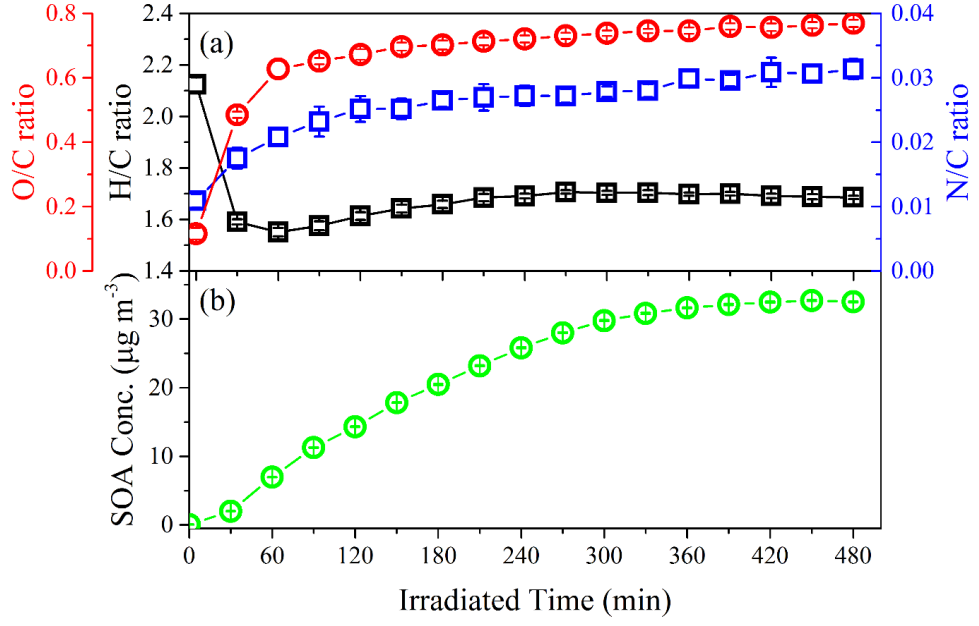

790

791 Fig. 8. Time evolution of (a) O/C, H/C and N/C and (b) SOA concentration in the photo-oxidation of gasoline vapor in the

792 presence of 150 ppb NH_3 (Exp. AGN1).

Atmos. Chem. Phys. Discuss., https://doi.org/10.5194/acp-2019-14
Manuscript under review for journal Atmos. Chem. Phys.
Discussion started: 16 January 2019

Atmospheric Chemistry and Physics Discussions

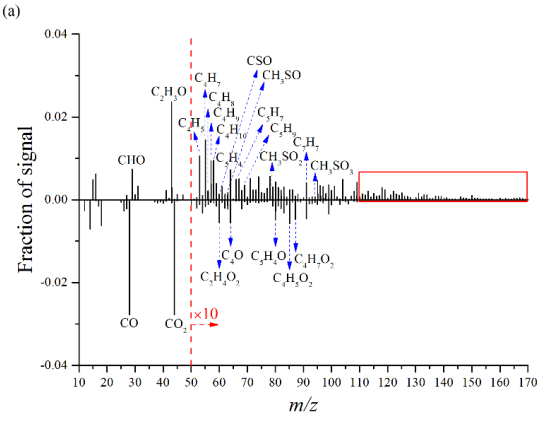

Fig. 9. (a) Difference mass spectra (Factor 1-S−Factor 2-S) between the two factors, (b) Time series of the mass concentration, and (c) Relationship between the concentration of SO_2 and the maximum concentration of the two factors identified by applying PMF analysis to the AMS data derived from the experiments at different concentrations of SO_2 (Exps. GN, SGN1,

Atmos. Chem. Phys. Discuss., https://doi.org/10.5194/acp-2019-14
Manuscript under review for journal Atmos. Chem. Phys.
Discussion started: 16 January 2019

799 SGN2, SGN3 and SGN4).

Atmos. Chem. Phys. Discuss., https://doi.org/10.5194/acp-2019-14
Manuscript under review for journal Atmos. Chem. Phys.
Discussion started: 16 January 2019

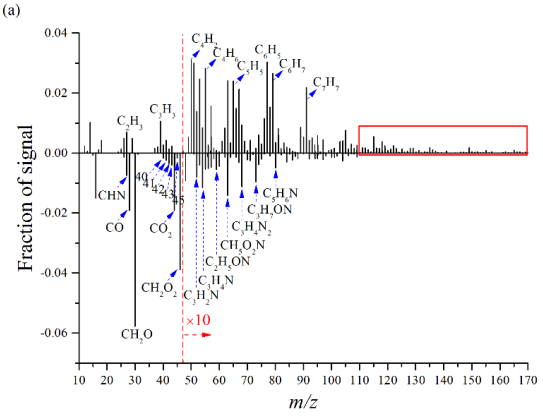

Fig. 10. (a) Difference mass spectra (Factor 1-N−Factor 2-N) between the two factors, (b) Time series of the mass concentration, and (c) Relationship between the concentration of NH_3 and the maximum concentration of the two factors identified by applying PMF analysis to the AMS data derived from the experiments at different concentrations of NH_3 (Exps. GN, AGN1

Atmos. Chem. Phys. Discuss., https://doi.org/10.5194/acp-2019-14
Manuscript under review for journal Atmos. Chem. Phys.
Discussion started: 16 January 2019

806 and AGN2).